arXiv:physics/0507015v1 [physics.optics] 2 Jul 2005

Electromagnetic modes in dielectric equilateral triangle resonators

G. M. Wysin*
Department of Physics
Kansas State University
Manhattan, KS 66506-2601
(Dated: July 1, 2005)

Resonant electromagnetic modes are analyzed inside a dielectric cavity of equilateral triangular cross section and refractive index n, surrounded by a uniform medium of refractive index n'. The field confinement is determined only under the requirements needed to maintain total internal reflection of the internal electromagnetic fields, matched to exponentially decaying evanescent waves outside the cavity. Two-dimensional electromagnetics is considered, with no dependence on the coordinate perpendicular to the cross section; hence, independent transverse electric (TE) and transverse magnetic (TM) polarizations are described separately. A linear combination of six plane waves is sufficient within the cavity, whose wavevectors are related by 120° rotations and whose phases are related by Fresnel reflection coefficients. Generally, the mode spectrum becomes sparse and the minimum mode frequency increases rapidly as the index ratio $\mathsf{N} = \mathsf{n}/\mathsf{n}'$ approaches 2. For specified quantum numbers and N, the TM modes are lower in frequency than the TE modes. Assuming the evanescent boundary waves escape at the triangle vertices, TE modes generally are found to have greater confinement of the fields inside the cavity and much higher quality factors than TM modes.

PACS numbers: 41.20.-q, 42.25.-p, 42.25.Gy, 42.60.-v, 42.60.Da
Keywords: equilateral triangle, resonator, total internal reflection, quality factor, lifetime

I. INTRODUCTION

Confinement of electromagnetic fields only by total internal reflection (TIR) offers a path for design of simple optical resonators or lasers with low volume and low threshold power. To this end, various two-dimensional (2D) geometries have been considered for their different influence on the mode properties, including disks,[1] cleaved[2] and etched[3] semiconductor triangles, squares,[4, 5, 6] and zeolite $ALPO_4$-5 hexagonal crystals.[7, 8] The problem of equilateral triangle resonators (ETR) considered here is particularly interesting, because the symmetry present allows for a considerable simplification of the analysis. Good estimates for the ETR mode wavefunctions, frequencies, and lifetimes (or quality factors) are developed here, based on a set of six plane waves within the resonator, matched to each other by Fresnel factors, producing exterior evanescent waves.

Chang *et al.*[2] analyzed the ETR wavefunctions under the assumption of Dirichlet boundary conditions (DBC), using an exactly known solution[9], for transverse magnetic (TM) polarization only. In the presence of a dielectric–dielectric boundary, however, the fields do not go to zero on the boundary, instead, the field confinement can be provided by TIR, assuming a refractive index in the cavity, n, greater than that of the surroundings, n'. Huang *et al.*[10, 11, 12] made a more complete analysis for an ETR with dielectric boundary conditions, approximately matching interior standing wave fields to exterior evanescent waves. Mode frequencies and quality factors Q were estimated[11] from 1000 to as high as 20000, using the finite-difference time-domain technique (FDTD) and Padé approximation[13], with the highest Q values associated with TM polarization. On the other hand, typical Q values from 20 – 150 were measured in photoluminescence (PL) experiments[3] on GaInAs-InP ETRs with edges from 5 – 20 μm. Recently I analyzed the ETR modes using the DBC approximation[14], and assuming the escape of evanescent boundary waves at the triangle vertices as the primary decay mechanism, estimated typical Q's from 10 – 500, with the highest values for TE polarization. Both of these theoretical approaches involve approximations, thus, it is important to consider an alternative description of the modes and clarify how the polarization influences the mode lifetimes.

The DBC approximation applied previously[2, 14] clearly does not describe the fields correctly at a dielectric–dielectric boundary. The goal here is to use the general knowledge of the modes from the DBC analysis, but do the correct matching of plane wave fields inside the cavity with evanescent fields on the outside. This matching is accomplished by employing the Fresnel reflection coefficients correctly for all the plane wave components present in the cavity. It is assumed that all the electromagnetic field components do not depend on a z-coordinate perpendicular to the triangular cross section (i.e., longitudinal wavevector $k_z = 0$). Then Maxwell's equations and associated dielectric boundary conditions lead to separated problems for TM and TE modes. Each polarization is controlled by one component of the electromagnetic field that must be continuous across the dielectric-dielectric boundary. For the TM modes, the controlling wavefunction is the longitudinal electric field, $\psi = E_z$; for TE modes, it is the longitudinal magnetic field, $\psi = H_z$.

*Electronic address: wysin@phys.ksu.edu; URL: `http://www.phys.ksu.edu/~wysin`

The exact solution for an ETR with Dirichlet boundary conditions is a superposition of six plane waves of equal strengths but different phases and wavevectors. The waves undergo a $-\pi$ phase shift when reflecting from the faces, as required such that the incident and reflected parts cancel exactly at the boundary. Any one of these waves, when followed through a sequence of reflections due to TIR, returns to its original direction after six reflections (see Fig. 1 of Ref. 14).

The situation is similar for the ETR with *dielectric boundary conditions* or *Maxwell boundary conditions* (MBC), where the correct field matching for Maxwell's equations must be applied. For either TE or TM polarization, I show that a combination of six plane waves is still needed within the cavity, related to each other by the reflections from the three cavity faces. For a resonant mode whose fields are TIR-confined within the cavity, all the waves must impinge on the faces at incident angles greater than the critical angle θ_c, where

$$\sin\theta_c = \frac{1}{\mathsf{N}}, \qquad \mathsf{N} = \frac{\mathsf{n}}{\mathsf{n}'}. \tag{1}$$

The generalization here compared to the DBC problem, is that when reflected from the faces, the waves undergo phase shifts determined by unit-modulus Fresnel coefficients, as well as being rotated in propagation direction. The goal here is to determine the correct wavevectors and complex amplitudes of these six plane waves such that a fully self-consistent wavefunction is determined.

When incident on the faces from inside the cavity, the waves produce evanescent waves in the exterior region just outside the cavity. It is difficult to give an exact description of the exterior fields, however, an approximate description is possible provided the six interior plane waves are incident on the cavity faces at angles sufficiently greater than θ_c. In that case, the penetration depth into the exterior region $d = |k'_\perp|^{-1}$, is much less than the cavity size or edge a. Then, there are only strong evanescent fields very close to the cavity, and a description of these based on the transmission amplitude via Fresnel's equations is appropriate. The mode lifetime and Q are estimated based on the assumption that the evanescent boundary waves radiate to the cavity surroundings when they reach the triangle vertices. This is a "strong damping" approximation, in the sense that the reflection or radiation of boundary wave energy back into the cavity is assumed to be insignificant.

The presentation proceeds as follows. First, the MBC field matching of the six plane waves is described. Equations for allowed quantum indexes are found, giving solutions for the mode wavevectors and wavefunctions. The wavefunction description is general enough that it describes equally well the DBC, TM and TE problems, or any other boundary condition whose reflection phase shift is determined by incident angle. Lifetimes will be estimated using the boundary wave radiation, and compared to the simpler DBC theory and other analysis.

II. EM FIELDS DESCRIPTION

A. Six interior plane waves

Here I describe the notation for the interior waves (ψ), with assumed frequency $\omega = c^* k$, where $c^* = c/\sqrt{\epsilon\mu}$ is the light speed in the cavity, and the wavevector modulus k is to be determined. The ETR has edge length a, and xy coordinates are used where the origin is set at its geometrical center, Fig. 1. An initial wave ① is supposed to emerge from lower edge b_0 at an angle $\alpha_1 = \alpha$ relative to the x-axis, and hence has wavevector components $\vec{k}_1 \equiv (k_x, k_y) = (k\cos\alpha, k\sin\alpha)$. Only certain values of α will lead to a solution for an eigenmode of the cavity; determination of the possible values of α is an essential part of the solution presented here.

This initial wave ① was formed by reflection of a wave incident on boundary b_0 at incident angle $\theta_{i,1} = 90^\circ - \alpha$. By consideration of the triangular geometry and using the law of reflection, it is seen that the incident angle when impinging on boundary b_1 will be $\theta_{i,2} = 60^\circ - \theta_{i,1}$, see Fig. 1. As the wave subsequently reflects from the boundaries in ordered sequence b_1, b_2, b_0, etc., the incident angles on each succeeding boundary simply oscillate between only two values symmetrically above and below 60°. Thus, without loss of generality, one can assume $\alpha \geq 60^\circ$ for the remaining analysis, and take k_x and k_y of wave ① as both positive. The sequence of waves generated from wave ①, by sequential reflections from b_1, b_2, b_0, b_1 and so on, are labeled as waves ②, ③, ④, ⑤ and ⑥. Finally, wave ⑥ emerges from b_2 and impinges on b_0 to regenerate an amplitude of wave ①. To produce a consistent solution, this regeneration of wave ① must be in phase with the original wave ①.

Considerations of the law of reflection together with the equilateral geometry leads to the basic properties of the six waves, as summarized in Table I. The xy components of each wavevector are defined from the α_l in the usual way,

$$\vec{k}_l = k(\cos\alpha_l, \sin\alpha_l). \tag{2}$$

It is seen that pairs of wavevectors, $[\vec{k}_1, \vec{k}_6]$, and $[\vec{k}_2, \vec{k}_3]$ and $[\vec{k}_4, \vec{k}_5]$, are related to each other by changing $\alpha \to -\alpha$. Each pair is related to the others by 120° counterclockwise rotations around the $\hat{z}$-axis, denoted by operator R, which can be represented by the square matrix,

$$R = \begin{pmatrix} -1/2 & -\sqrt{3}/2 \\ \sqrt{3}/2 & -1/2 \end{pmatrix}. \tag{3}$$

The pair $[\vec{k}_1, \vec{k}_6]$ can be considered the original waves, from which the others are obtained. Wavevector $\vec{k}_6$ is simply obtained from $\vec{k}_1$ by reflection across the $\hat{x}$-axis.

Due to the triangular symmetry, and the unit-modulus reflection coefficient under TIR, all six waves must have equal magnitudes, but different phases. Then the net

TABLE I: Definitions of the parameters of the plane waves labeled by wavevectors $\vec{k}_l$, within the triangular cavity. α_l is the angle that each $\vec{k}_l$ makes to the x-axis. R is the operator for rotation through $+120^\circ$ around the $\hat{z}$-axis.

	①	②	③	④	⑤	⑥
$\alpha_l =$	α	$-\alpha+240^\circ$	$\alpha+240^\circ$	$-\alpha+120^\circ$	$\alpha+120^\circ$	$-\alpha$
$\vec{k}_l =$	$\vec{k}_1$	$R^2\cdot\vec{k}_6$	$R^2\cdot\vec{k}_1$	$R\cdot\vec{k}_6$	$R\cdot\vec{k}_1$	$\vec{k}_1(-\alpha)$

wavefunction within the cavity is written as a sum over the waves

$$\psi = \sum_{l=1}^{6} A_l e^{i\vec{k}_l\cdot\vec{r}} \tag{4}$$

where the A_l are all of unit modulus, and $\psi = H_z$ for TE modes or $\psi = E_z$ for TM modes. In both polarizations, ψ must be continuous across the cavity boundary. The TE and TM wavefunctions will not be the same, however, due to the different phase shifts implied by the Fresnel factors.

Now consider what happens to these waves in terms of their interaction with the lower boundary, b_0, which lies parallel to $\hat{x}$ at $y = -a/(2\sqrt{3})$. By appropriate symmetry transformations, the effects on the other two boundaries can be inferred. Three of the waves must be receding from b_0 and three must be approaching b_0. Using the fact that $60^\circ \le \alpha < 90^\circ$, for example, writing $\alpha = 60^\circ + \vartheta$, where $\vartheta < 30^\circ$, the respective angles of the $\vec{k}_l$ to the $\hat{x}$-axis are $60^\circ - \vartheta$, $180^\circ - \vartheta$, $-60^\circ + \vartheta$, $60^\circ - \vartheta$, $180^\circ + \vartheta$, and $-60^\circ - \vartheta$. Those that fall in the range from 0° to -180° (including shifts by multiples of 360°) are incident on b_0. Thus, the waves ③, ⑤ and ⑥ are incident on b_0. Their incident angles are obtained from the formula, $\theta_i = 90^\circ + \alpha_l$, as -90° is the outward normal direction to b_0. Then waves ③, ⑤ and ⑥ have incident angles on b_0,

$$\theta_{i,3} = \alpha - 30^\circ, \quad \theta_{i,5} = \alpha - 150^\circ, \quad \theta_{i,6} = 90^\circ - \alpha. \tag{5}$$

One sees that $\theta_{i,6}$ always has the smallest magnitude. $\theta_{i,5}$ is less than zero because wave ⑤ has a negative wavevector component along $\hat{x}$.

Extending such arguments to the other faces, the ray diagram of Fig. 1 summarizes the results, showing the incident angles of all the waves on each of the faces. It is important to notice that the only incident angles in the problem are the three of Eq. 5. For example, wave ① is incident on b_1, but at incident angle $\theta_{i,3}$. The symmetries represented in Fig. 1 will be exploited to determine the correct wave amplitudes.

B. Field matching at the dielectric interface – Maxwell boundary conditions

Now consider the reflections of the waves ③, ⑤, and ⑥ from b_0, starting with wave ⑥. When wave ⑥ impinges on b_0, its reflection regenerates wave ① and it also produces an exterior evanescent wave, denoted ⑥′, of amplitude F_6 (measured on the boundary) and wavevector $\vec{k}_6'$, with $k_{6',x} = k_{6,x}$ by Snell's Law. Ignoring the other interior waves, we match incident wave ⑥ and reflected wave ① to the exterior evanescent wave, ⑥′. Matching the net ψ at $y = -a/(2\sqrt{3})$, we have terms all proportional to the common phase factor, $e^{i(k_x x-\omega t)}$, where $k_x = k\cos\alpha$,

$$A_6 e^{ik_{6y}\cdot(\frac{-a}{2\sqrt{3}})} + A_1 e^{ik_{1y}\cdot(\frac{-a}{2\sqrt{3}})} = F_6. \tag{6}$$

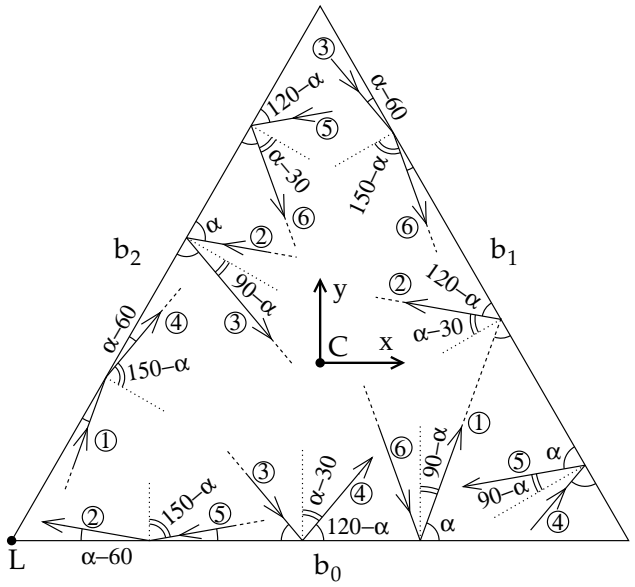

FIG. 1: xy coordinates, with origin at triangle center, and boundaries b_0, b_1 and b_2. Rays represent the six planes waves propagating within the cavity, sketched for the value, $\alpha = 70^\circ$. The plane wave incident angles here determine the reflection amplitudes and phases used in Table II.

TABLE II: Relations between the incident and reflected wave amplitudes on the lower boundary (b_0), the upper right boundary (b_1) and the upper left boundary (b_2). The net reflection phase shifts are $\Delta_l = \delta_l - k_{ly}\frac{a}{\sqrt{3}}$, where $\delta_l = \delta(\theta_{i,l})$ is the Fresnel reflection phase shift. See Fig. 1 for the geometrical reasoning behind this table.

boundary	incident	θ_i	reflected
b_0	③, A_3	$\theta_{i,3} = \alpha - 30^\circ$	④, $A_4 = A_3 e^{i\Delta_3}$
b_0	⑤, A_5	$\theta_{i,5} = \alpha - 150^\circ$	②, $A_2 = A_5 e^{i\Delta_5}$
b_0	⑥, A_6	$\theta_{i,6} = 90^\circ - \alpha$	①, $A_1 = A_6 e^{i\Delta_6}$
b_1	①, A_1	$\theta_{i,3}$	②, $A_2 = A_1 e^{i\Delta_3}$
b_1	③, A_3	$\theta_{i,5}$	⑥, $A_6 = A_3 e^{i\Delta_5}$
b_1	④, A_4	$\theta_{i,6}$	⑤, $A_5 = A_4 e^{i\Delta_6}$
b_2	⑤, A_5	$\theta_{i,3}$	⑥, $A_6 = A_5 e^{i\Delta_3}$
b_2	①, A_1	$\theta_{i,5}$	④, $A_4 = A_1 e^{i\Delta_5}$
b_2	②, A_2	$\theta_{i,6}$	③, $A_3 = A_2 e^{i\Delta_6}$

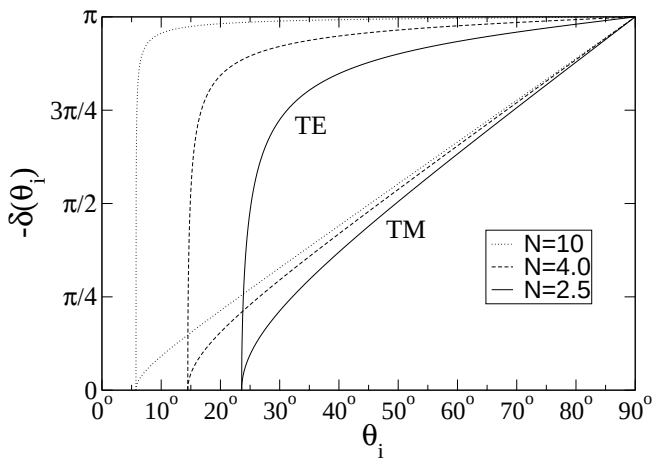

FIG. 2: Dependence of the TIR Fresnel reflection phase shifts on incident angle, for TM [Eq. (38)] and TE [Eq. (40)] polarization at the indicated refractive index ratios N, assuming unit magnetic permeabilities.

On the other hand, in the usual analysis of the reflection, the correct boundary conditions for Maxwell's equations will relate the incident ($\psi_{\rm inc.}$) and reflected ($\psi_{\rm refl.}$) amplitudes, *measured at the boundary*, by a Fresnel reflection factor $r(\theta_i)$,

$$\frac{\psi_{\rm refl.}}{\psi_{\rm inc.}} = r(\theta_i) = e^{i\delta(\theta_i)}. \tag{7}$$

Here $\delta(\theta_i)$ is the phase shift experienced by the wave upon reflection, for incident angle θ_i, in conditions of TIR. The θ_i-dependence of the different Fresnel factors appearing for TE and TM polarization is discussed subsequently in Sec. III, see Fig. 2 for typical dependence with dielectric boundary conditions.

Expressions (6) and (7) imply that the wave amplitudes A_6 and A_1 have a relation,

$$r_6 = e^{i\delta_6} = \frac{A_1 e^{-ik_{1y}\frac{a}{2\sqrt{3}}}}{A_6 e^{-ik_{6y}\frac{a}{2\sqrt{3}}}} = \frac{A_1}{A_6} e^{ik_{6y}\frac{a}{\sqrt{3}}}. \tag{8}$$

The phase factor involves the y-component of $\vec{k}_6$, which is the negative of the y-component of $\vec{k}_1$. The subscripts on r and δ indicate evaluating at the incident angle for wave ⑥, $\theta_{i,6} = 90° - \alpha$. This allows us to write the reflected and evanescent field amplitudes in terms of A_6,

$$A_1 = A_6 e^{i\delta_6} e^{-ik_{6y}\frac{a}{\sqrt{3}}}, \quad F_6 = A_6(1+e^{i\delta_6})e^{-ik_{6y}\frac{a}{2\sqrt{3}}}. \tag{9}$$

An equivalent algebra applies for analyzing how wave ⑤ incident on b_0 produces reflected wave ②, and an exterior evanescent wave ⑤′, in terms of incident angle $\theta_{i,5} = \alpha - 150°$, and associated phase shift, δ_5. The reflected and exterior field amplitudes are

$$A_2 = A_5 e^{i\delta_5} e^{-ik_{5y}\frac{a}{\sqrt{3}}}, \quad F_5 = A_5(1+e^{i\delta_5})e^{-ik_{5y}\frac{a}{2\sqrt{3}}}. \tag{10}$$

Finally, wave ③ incident on b_0 produces reflected wave ④ and evanescent wave ③′, with similar expressions,

$$A_4 = A_3 e^{i\delta_3} e^{-ik_{3y}\frac{a}{\sqrt{3}}}, \quad F_3 = A_3(1+e^{i\delta_3})e^{-ik_{3y}\frac{a}{2\sqrt{3}}}. \tag{11}$$

The same type of analysis can be applied to the waves incident on boundaries b_1 and b_2, using the incident angles seen in Fig. 1. One can also use the symmetries under 120° rotations R, seeing that, for example, $R \cdot b_0 = b_1$, and $R \cdot \vec{k}_6 = \vec{k}_4$, $R \cdot \vec{k}_1 = \vec{k}_5$, implying that the phase relationship between waves ⑥ and ① on b_0 is the same as the relationship between ④ and ⑤ on b_2. Similar arguments apply to the other pairs of waves. The results of this analysis are summarized in Table II, where the phase factors relating the wave amplitudes are denoted by

$$\Delta_l \equiv \delta_l - k_{ly}\frac{a}{\sqrt{3}}, \qquad l = 3, 5, 6. \tag{12}$$

There are only three distinct incident angles in the problem, corresponding to the three fundamental θ_i of Eq. 5. These factors Δ_3, Δ_5 and Δ_6 are now the only quantities needed to correctly match self-consistently the interior fields, according to the nine equations in the last column of Table II.

III. DETERMINATION OF THE RESONANT FREQUENCIES AND WAVEFUNCTIONS

The nine equations in the Table II can be summarized as three basic ratios,

$$\frac{A_4}{A_3} = \frac{A_2}{A_1} = \frac{A_6}{A_5} = e^{i\Delta_3}, \tag{13a}$$

$$\frac{A_2}{A_5} = \frac{A_6}{A_3} = \frac{A_4}{A_1} = e^{i\Delta_5}, \tag{13b}$$

$$\frac{A_1}{A_6} = \frac{A_5}{A_4} = \frac{A_3}{A_2} = e^{i\Delta_6}, \tag{13c}$$

Due to the simple structure, one sees the relation

$$\frac{A_2 A_4 A_6}{A_1 A_3 A_5} = e^{i3\Delta_3} = e^{i3\Delta_5} = e^{-i3\Delta_6}. \tag{14}$$

This leads to two fundamental relations for these phases,

$$e^{i3(\Delta_3+\Delta_6)} = 1, \qquad e^{i3(\Delta_5+\Delta_6)} = 1. \tag{15}$$

Using all of the equations (13) together gives the relation,

$$e^{i(\Delta_3+\Delta_5+2\Delta_6)} = 1. \tag{16}$$

Although these last three relations are not linearly independent, all are required to describe the solution. The

first two imply introduction of some integers denoted as n_3 and n_5, such that

$$\Delta_3 + \Delta_6 = \frac{2\pi}{3} n_3, \qquad \Delta_5 + \Delta_6 = \frac{2\pi}{3} n_5. \tag{17}$$

Eq. (16) leads to, on the other hand,

$$\Delta_3 + \Delta_5 + 2\Delta_6 = 2\pi n_6, \tag{18}$$

where n_6 must also be an integer. Comparing these equations demonstrates the constraint,

$$n_3 + n_5 = 3n_6, \tag{19}$$

that is, the sum of n_3 and n_5 must be a multiple of 3. However, not all possible choices of these integers will lead to allowed solutions. Once the allowed quantum numbers n_3 and n_5 are determined, the amplitude ratios of the six plane waves will be determined.

Eqs. (17) and (18) merely give some sums of the Δ_l phase factors, whereas, we actually need to determine each one separately, and more importantly, we need to find the wavevector magnitude k. This is accomplished by using their definitions (12) together with the corresponding y-components of the wavevectors, obtained from (2). The necessary components are

$$k_{3y} = k\sin(\alpha - 120^\circ) = -\frac{k}{2}(\sin\alpha + \sqrt{3}\cos\alpha), \tag{20a}$$

$$k_{5y} = k\sin(\alpha + 120^\circ) = -\frac{k}{2}(\sin\alpha - \sqrt{3}\cos\alpha), \tag{20b}$$

$$k_{6y} = k\sin(-\alpha) = -k\sin\alpha. \tag{20c}$$

Then this leads to the Δ_l combinations,

$$\Delta_3 + \Delta_6 = (\delta_3 + \delta_6) + \frac{1}{2}ka(\sqrt{3}\sin\alpha + \cos\alpha), \tag{21a}$$

$$\Delta_5 + \Delta_6 = (\delta_5 + \delta_6) + \frac{1}{2}ka(\sqrt{3}\sin\alpha - \cos\alpha), \tag{21b}$$

$$\Delta_3 + \Delta_5 + 2\Delta_6 = (\delta_3 + \delta_5 + 2\delta_6) + \sqrt{3}\; ka\sin\alpha. \tag{21c}$$

The last of these then determines $k_y \equiv k_{1y} = k\sin\alpha$. Another combination involves only $k_x \equiv k_{1x} = k\cos\alpha$,

$$\Delta_3 - \Delta_5 = (\delta_3 - \delta_5) + ka\cos\alpha = \frac{2\pi}{3}(n_3 - n_5). \tag{22}$$

Then the basic wavevector components of wave ① are expressed as

$$k_x a = ka\cos\alpha = \frac{2\pi}{3}(n_3 - n_5) - (\delta_3 - \delta_5), \tag{23a}$$

$$k_y a = ka\sin\alpha = \frac{1}{\sqrt{3}}\left[2\pi n_6 - (\delta_3 + \delta_5 + 2\delta_6)\right]. \tag{23b}$$

Remembering that the Fresnel phase shifts $\delta(\theta_{i,l})$ depend ultimately on α, via equations (5), the Eqs. (23) are seen to be coupled transcendental equations for unknowns k and α, assuming n_3 and n_5 are given. They can be solved in various ways. A simple approach is to eliminate k, and then determine the allowed α as the roots of the following function,

$$\begin{aligned} p(\alpha) \;&=\; \left[\frac{2\pi}{3}(n_3 + n_5) - (\delta_3 + \delta_5 + 2\delta_6)\right]\cos\alpha \\ &-\; \sqrt{3}\left[\frac{2\pi}{3}(n_3 - n_5) - (\delta_3 - \delta_5)\right]\sin\alpha = 0. \end{aligned} \tag{24}$$

In this last expression n_6 was eliminated using the constraint (19). In the general case, it is not possible to solve for α in closed form. On the other hand, some straightforward analysis of this function, together with numerical evaluation indicates the region in which to look for the quantum numbers n_3 and n_5.

Once α has been determined, the modulus of the mode's wavevector, k, can be found from either (23a) or (23b), or by their combination, written in a form like that for the known solution for the DBC case [Eq. (35)],

$$\begin{aligned} ka = \frac{2\pi}{3}\;\Big\{\;&\Big[n_3 - n_5 - \frac{3}{2\pi}(\delta_3 - \delta_5)\Big]^2 \\ &+3\Big[n_6 - \frac{1}{2\pi}(\delta_3 + \delta_5 + 2\delta_6)\Big]^2\Big\}^{1/2}. \end{aligned} \tag{25}$$

A. The resonant wavefunctions

Assuming α has been found (see below for DBC, TE and TM cases), then k_x, k_y, and k or $\omega = c^*k$ are determined. In addition, Eqs. (12) determine the phase factors needed to express the complete wavefunction for any mode, in terms of α via Eqs. (23) and (5). The quantum numbers and Fresnel phase shifts give the Δ_l as

$$\Delta_3 = \frac{1}{3}\left[\frac{2\pi}{3}(2n_3 - n_5) + (\delta_3 + \delta_5 - \delta_6)\right], \tag{26a}$$

$$\Delta_5 = \frac{1}{3}\left[\frac{2\pi}{3}(2n_5 - n_3) + (\delta_3 + \delta_5 - \delta_6)\right], \tag{26b}$$

$$\Delta_6 = \frac{1}{3}\left[\frac{2\pi}{3}(n_3 + n_5) - (\delta_3 + \delta_5 - \delta_6)\right], \tag{26c}$$

all of which depend on a net phase factor,

$$\varphi(\alpha) \equiv \delta_3 + \delta_5 - \delta_6. \tag{27}$$

This allows evaluation of the wavefunction (4), simplified by freely choosing the amplitude of wave ① as

$$A_1 = \frac{1}{2}A_0 \exp\left\{-i\left[\frac{2\pi}{9}(n_3+n_5)+\frac{1}{6}\varphi\right]\right\}, \qquad (28)$$

where A_0 is the overall wavefunction amplitude.

$$\begin{aligned}\psi \;&= A_0\left\{e^{ik_x x}\cos\left[k_y y-\frac{2\pi}{9}(n_3+n_5)-\frac{1}{6}\varphi\right]\right.\\ &+\; e^{ik_{3x}x}\cos\left[k_{3y}y-\frac{2\pi}{9}(n_5-2n_3)-\frac{1}{6}\varphi\right]\\ &+\; \left.e^{ik_{5x}x}\cos\left[k_{5y}y-\frac{2\pi}{9}(n_3-2n_5)-\frac{1}{6}\varphi\right]\right\}, \qquad (29)\end{aligned}$$

where the wavevectors of waves ①, ③, and ⑤ are needed, e.g., from Eqs. (23) and using Table I,

$$k_{3x} = -\frac{1}{2}k_x + \frac{\sqrt{3}}{2}k_y, \qquad k_{3y} = -\frac{\sqrt{3}}{2}k_x - \frac{1}{2}k_y. \qquad (30)$$

$$k_{5x} = -\frac{1}{2}k_x - \frac{\sqrt{3}}{2}k_y, \qquad k_{5y} = \frac{\sqrt{3}}{2}k_x - \frac{1}{2}k_y, \qquad (31)$$

Note that if $\alpha = 60°$, then $\theta_{i,3} = \theta_{i,6} = 30°$, making $\delta_3 = \delta_6$, and hence, $\varphi = \delta_5 = -\pi$ (grazing incidence for wave ⑤, TE or TM polarization). Putting $\alpha = 60°$ also gives $n_3 = 2n_5 + 3$ (See III B below). These values cause the wavefunction ψ to vanish; there are no modes with $\alpha = 60°$ for the DBC, TE or TM cases, although it is tempting to sketch such ray diagrams.

B. Equilateral triangle cavity with Dirichlet boundary conditions

It is interesting to check the validity of the six-wave analysis in the case of Dirichlet boundary conditions; this also helps to locate the allowed n_3 and n_5 for Maxwell boundary conditions. The net field on the boundary becomes zero when the Fresnel phase shifts are all taken to be $\delta_l = -\pi$ (this is the limiting phase shift for grazing incidence, in either TE or TM polarization). Then the wavevector components reduce to

$$k_x a = \frac{2\pi}{3}(n_3 - n_5), \qquad k_y a = \frac{2\pi}{\sqrt{3}}(n_6 + 2). \qquad (32)$$

The original assumption, $\alpha \geq 60°$, imposes the relation $\tan\alpha = k_y/k_x \geq \sqrt{3}$. At the limiting value $\alpha = 60°$, however, the net wavefunction ψ of Eq. (29) vanishes; $\alpha = 60°$ is not allowed. There results $n_3 < 2n_5 + 3$ (equality maps to $\alpha = 60°$). Also it was implicitly assumed that $k_x \geq 0$, hence, we require $n_3 \geq n_5$. Therefore, a given choice of n_5 allows a limited range of n_3,

$$n_5 \leq n_3 < 2n_5 + 3. \qquad (33)$$

Using values $n_5 \geq 0$ and evaluating the possible quantum numbers, the well-known solutions for DBC are recovered[2, 9, 15], in terms of shifted quantum numbers,

$$m \equiv (n_3 - n_5), \qquad n \equiv (n_6 + 2). \qquad (34)$$

These must be both odd, or both even, with the restriction $m < n$. Generally, we use these quantum numbers to label the modes with dielectric boundary conditions, in place of n_3, n_5. Then the DBC wavevector moduli are reproduced from (25),

$$ka = \frac{2\pi}{3}\{m^2 + 3n^2\}^{1/2}. \qquad (35)$$

Note that the prohibited solutions at $\alpha = 60°$ would correspond to the prohibited case, $m = n$. It is straightforward to check that the $(m < n)$ DBC wavefunctions vanish on all the boundaries.

C. Maxwell boundary conditions: TM or TE polarization

To define Eq. (24) for $p(\alpha) = 0$, we require the Fresnel phase shifts for MBC. For TM polarization, $\psi = E_z$, and the Fresnel reflection coefficient for electric field polarized perpendicular to the plane of incidence is needed. For incident angle θ_i, the formula is[16]

$$\frac{\psi_{\text{refl.}}}{\psi_{\text{inc.}}} = e^{i\delta} = \frac{\sqrt{\frac{\epsilon}{\mu}}\cos\theta_i - \sqrt{\frac{\epsilon'}{\mu'}}\cos\theta'}{\sqrt{\frac{\epsilon}{\mu}}\cos\theta_i + \sqrt{\frac{\epsilon'}{\mu'}}\cos\theta'} \qquad \text{(TM)}. \quad (36)$$

Unprimed electric permittivity ϵ and magnetic permeability μ correspond to the cavity medium, whereas the primed values are those outside the cavity; the refractive indexes result from $\mathsf{n} = \sqrt{\epsilon\mu}$. Angle θ' is the refraction angle, a complex quantity obtained from Snell's Law under TIR,

$$\cos\theta' = i\gamma' \equiv i\sqrt{(\sin\theta_i/\sin\theta_c)^2 - 1}, \qquad (37)$$

where critical angle θ_c is defined in Eq. (1). The phase shift can be expressed also via

$$\tan\frac{\delta}{2} = -\frac{\mu}{\mu'}\sqrt{\frac{\cos^2\theta_c}{\cos^2\theta_i} - 1} \qquad \text{(TM)}. \qquad (38)$$

In the usual case for many optical materials with $\mu \approx \mu' \approx 1$, the phase shift changes slowly as θ_i ranges from θ_c ($\delta = 0$) to 90° ($\delta = -\pi$). Typical examples for index ratio $\mathsf{N} = 2.5, 4.0, 10.0$ are shown in Fig. 2. In numerical results presented here we assume $\mu = \mu' = 1$, as for most optical materials.

For TE polarization, $\psi = H_z$, and the Fresnel reflection coefficient for electric field polarized within the plane

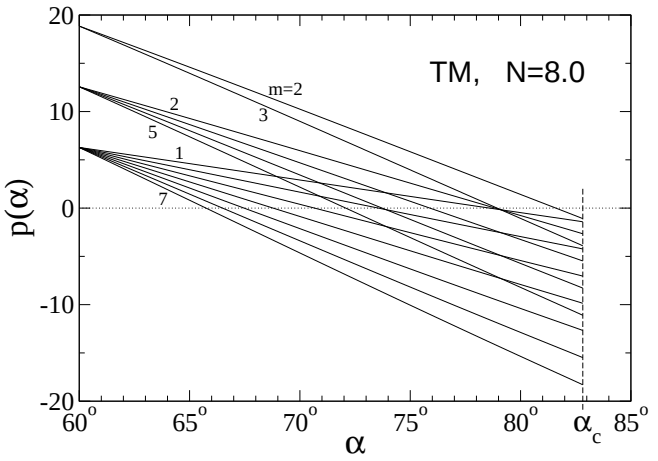

FIG. 3: Example $p(\alpha)$ functions [Eq. (24)] at $\mathsf{N} = 8$, $\mu = \mu'$, for TM polarization, giving the lowest 13 valid mode solutions, located by zero crossings (dotted line). The individual curves are labeled by (m, n), see Eq. (34), where m changes in unit increments. There are three different groupings of curves. The bottom group (7 curves) has $n - m = 2$, the middle group has $n - m = 4$, and the top group has $n - m = 6$. The values at the left limit are $p(60^\circ) = (n - m)\pi$. The right limiting point is $\alpha_c = 90^\circ - \theta_c$.

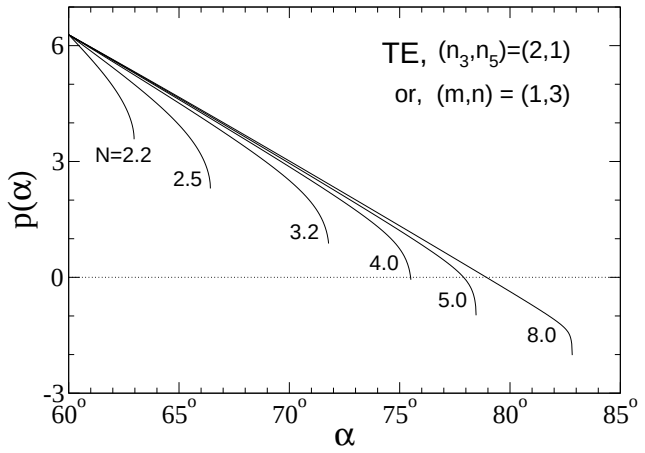

FIG. 4: Example $p(\alpha)$ functions for TE polarization, with the quantum numbers fixed at their lowest nonzero values, for various indicated index ratios N. Only the curves which cross zero (dotted line) give valid mode solutions ($\mathsf{N} \gtrsim 4$). The different termination points of the curves occur at $\alpha_c = 90^\circ - \theta_c$.

of incidence is needed. The Fresnel formula is[16]

$$\frac{\psi_{\rm refl.}}{\psi_{\rm inc.}} = e^{i\delta} = \frac{\sqrt{\frac{\epsilon'}{\mu'}}\cos\theta_i - \sqrt{\frac{\epsilon}{\mu}}\cos\theta'}{\sqrt{\frac{\epsilon'}{\mu'}}\cos\theta_i + \sqrt{\frac{\epsilon}{\mu}}\cos\theta'} \qquad \text{(TE)}. \quad (39)$$

Equivalently, the reflection phase shift is given by

$$\tan\frac{\delta}{2} = -\frac{\epsilon}{\epsilon'}\sqrt{\frac{\cos^2\theta_c}{\cos^2\theta_i} - 1} \qquad \text{(TE)}. \quad (40)$$

The important difference, in comparison with that for TM polarization, is the presence of the factor ϵ/ϵ' instead of μ/μ'. This significantly enhances the initial rate at which δ increases with θ_i, as can be seen in Fig. 2. Both the TM and TE phases shifts reach $-\pi$ at $\theta_i = 90^\circ$, but for TE the approach is much more rapid. This can also be taken to imply that a DBC approximation for the modes, such as that applied in Ref. 14, is more reasonable for TE modes than for TM modes.

D. Mode solutions: determination of α and (n_3, n_5) pairs, Maxwell boundary conditions

Now consider the solution of Eq. (24) for α under MBC. As shown earlier, there are no solutions with $\alpha = 60^\circ$, because such a choice causes the wavefunction (29) to vanish. The other extreme, $\alpha = 90^\circ$, which requires $n_3 = n_5$, is prohibited because wave ⑥ can never experience TIR at a vanishing incident angle. Then, for

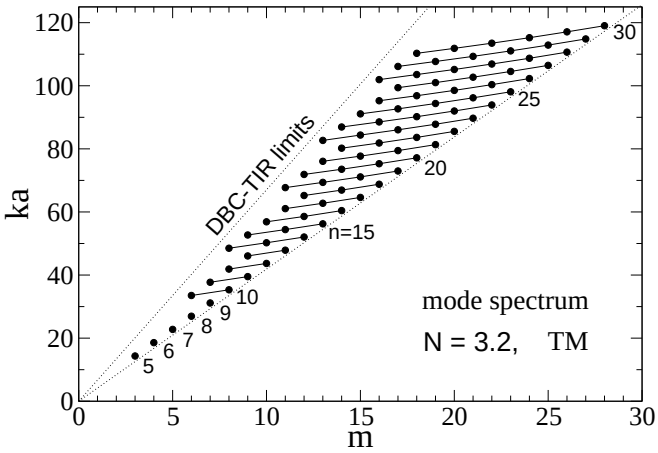

FIG. 5: The lowest mode wavevectors for TM polarization at index ratio $\mathsf{N} = 3.2$, plotted versus quantum index $m = n_3 - n_5$, for different values of the other index $n = n_6 + 2$ (Eq. 34) indicated next to the curves, changing by unit increments. The solid circles indicate allowed modes; the solid lines connect those having equal values of n. The dotted lines locate the limits of stable TIR as expected from using the DBC solution for the ETR, Eqs. (45) and (46), explained in the text.

MBC, similar to Eq. (33), the search for possible (n_3, n_5) pairs must take place in the range

$$n_5 < n_3 < 2n_5 + 3. \quad (41)$$

It is straightforward to calculate $p(\alpha)$ [Eq. (24)] numerically and determine the zero crossings, which only take place provided that n_3 is fairly close to the upper limit of (41). Choices of n_3, n_5 were made as follows. Starting from some $n_5 \geq 0$, calculate $n_3 = 2n_5 + 3$, which gives a prohibited pair at $\alpha = 60^\circ$. Automatically the

sum $(n_3 + n_5)$ is a multiple of 3. Then the first pair to check for a valid solution, is to take n_3 reduced by 1 ($n_3 \to n_3 - 1$) and n_5 increased by 1 ($n_5 \to n_5 + 1$), such that the sum is the same multiple of 3. The resulting pair (n_3, n_5) will likely have a solution for α if n_5 is adequately large. This initial pair is equivalently set by

$$n_3 = 2n_5, \qquad n_5 = 1, 2, 3 \ldots \tag{42}$$

Other pairs to try are found by continuing the reduction of n_3 by 1 together with the incrementing of n_5 by 1.

The solution for α must occur within the range

$$60^\circ < \alpha < 90^\circ - \theta_c, \tag{43}$$

because the incident angle of wave ⑥, $\theta_{i,6} = 90^\circ - \alpha$, cannot surpass the critical angle. Therefore, there is a considerably larger range for possible solutions for α as the index ratio increases (smaller θ_c). Conversely, an index ratio only slightly above 2.0 makes a substantially limited search range for α, as a result, fairly large values of n_5 are required before a solution is found.

Plots of $p(\alpha)$ are surprisingly close to linear, especially for larger index ratio N and TM polarization. Examples are shown in Fig. 3 for index ratio N = 8, with various (n_3, n_5) pairs [or in terms of (m, n)] and TM polarization. One should note that the various $p(\alpha)$ curves at different quantum numbers are closely related; the obvious visible change occurs in the typical slopes as n_3 and n_5 are adjusted, while the $\delta_i(\alpha)$ do not change. The dependence of some $p(\alpha)$ curves on N is indicated in Fig. 4, at fixed $(n_3, n_5) = (2, 1)$ for TE polarization. The terminating points of these curves occur at $\alpha_c = 90^\circ - \theta_c$. Then, the possibility for a zero crossing is greatly enhanced as N increases. Similar plots for TM polarization show curves much closer to linear form. The strong downward curvature as $\alpha \to \alpha_c$ for TE polarization means that for given quantum numbers, a TE polarized mode can be excited at lower index ratio than the same TM mode.

IV. CALCULATIONS OF MODE SPECTRA AND PROPERTIES

Having found (n_3, n_5) pairs and associated α, we can look at the mode dependence on polarization and refractive index ratio N. Henceforth, modes will be labeled by the quantum number pairs, (m, n).

A. TM polarization

For TM polarization, the frequencies of the lowest modes are displayed in Fig. 5 for N = 3.2, in terms of their dependences on the mode indexes (m, n), defined in Eq. (34). This value for index ratio was used in Ref. 17 in numerical and experimental studies of ETR semiconductor cavities, with a different theoretical analysis of the modes. In general, the trend is for ka to increase with

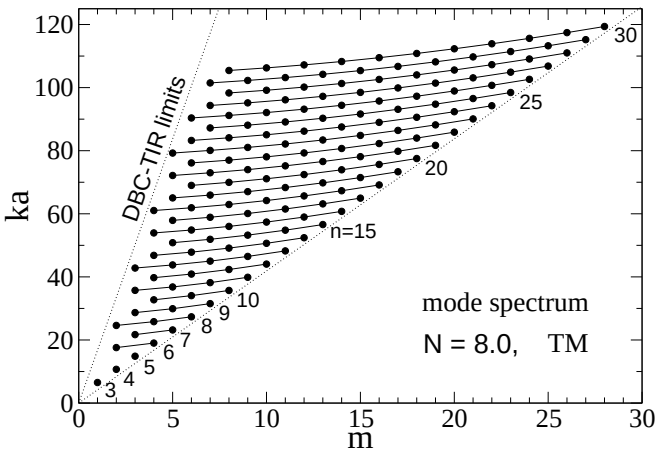

FIG. 6: The lowest mode wavevectors for TM polarization at index ratio N = 8.0, plotted as described in Fig. 5. Note also that the fundamental mode here has lower (m, n) and ka than that for N = 3.2 .

increasing quantum numbers. Just as in the DBC analysis, the allowed modes for MBC must have indexes m and n either both odd, or both even (parity constraint). Note, however, that the TM mode wavevectors for chosen (m, n) are noticeably lower than the values expected from the simplified DBC theory, expression (35), see Figs. 9 and 13 below. This can be attributed to the fact that the reflection phase shifts [from (38)] due not tend towards $-\pi$ even at very large index ratio N.

The positions of the ka upper limits (see dotted lines in Fig. 5) can be estimated quite accurately by using the TIR cutoff for a mode from the DBC theory[14]. Using the DBC solutions, all six plane waves can maintain TIR at all the boundaries only when

$$m > n\sqrt{\frac{3}{\mathsf{N}^2 - 1}}. \tag{44}$$

Combining this with Eq. (35) for ka leads to the DBC-TIR limiting curve, expected to hold reasonably well at higher index ratio,

$$ka = \frac{\omega a}{c^*} < \frac{2\pi \mathsf{N}}{3} m. \tag{45}$$

Additionally, the right limiting points of each curve correspond to quantum index pairs with $n = m+2$, or equivalently, $n_3 = 2n_5$. Then also using the DBC wavevectors (35), together with constraint $m < n$, valid for either DBC or MBC, leads to the ka lower limit,

$$ka = \frac{\omega a}{c^*} > \frac{4\pi}{3} m. \tag{46}$$

Indeed, all the results for Maxwell boundary conditions lie between these results, the dotted lines in Fig. 5, lending support to general aspects of the DBC theory.

As N is increased, the lower TIR limit does not change, while the DBC-TIR upper limit moves steeper, or to the

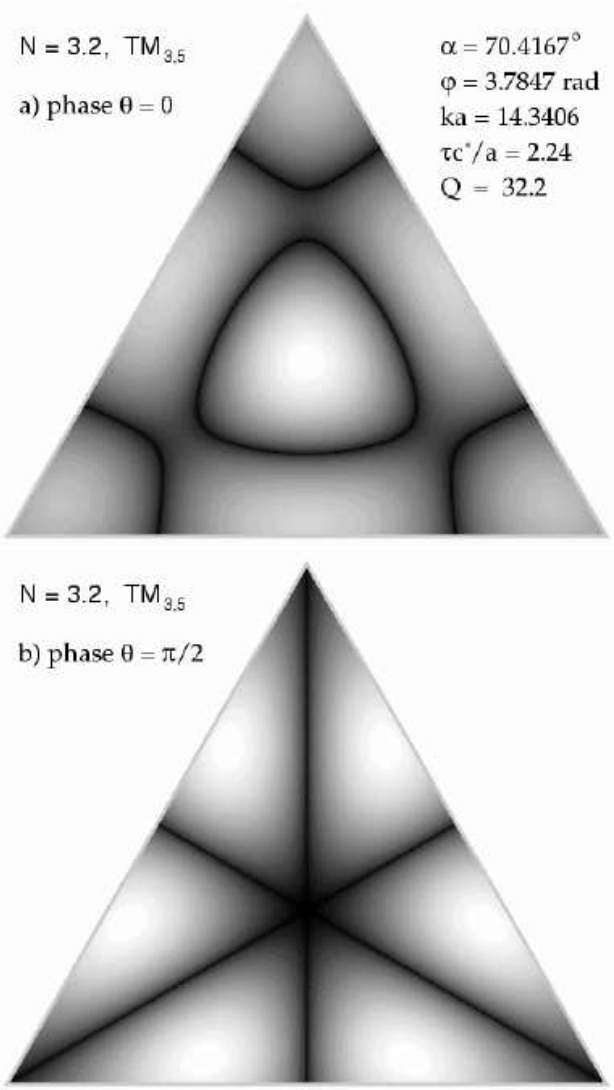

FIG. 7: Fundamental TM modes of oscillation at $\mathsf{N} = 3.2$, with $(m, n) = (3, 5)$, where the pixel intensity is proportional to $|Re\{\psi\}|^{1/2}$, which enhances the definition of the nodal curves. The black nodal curves separate alternating regions of positive and negative $Re\{\psi\}$. Two degenerate wavefunctions are displayed. In a) phase is $\theta_0 = 0$, in b) the phase is $\theta_0 = \pi/2$, where the mode amplitude is $A_0 = e^{i\theta_0}$, see text.

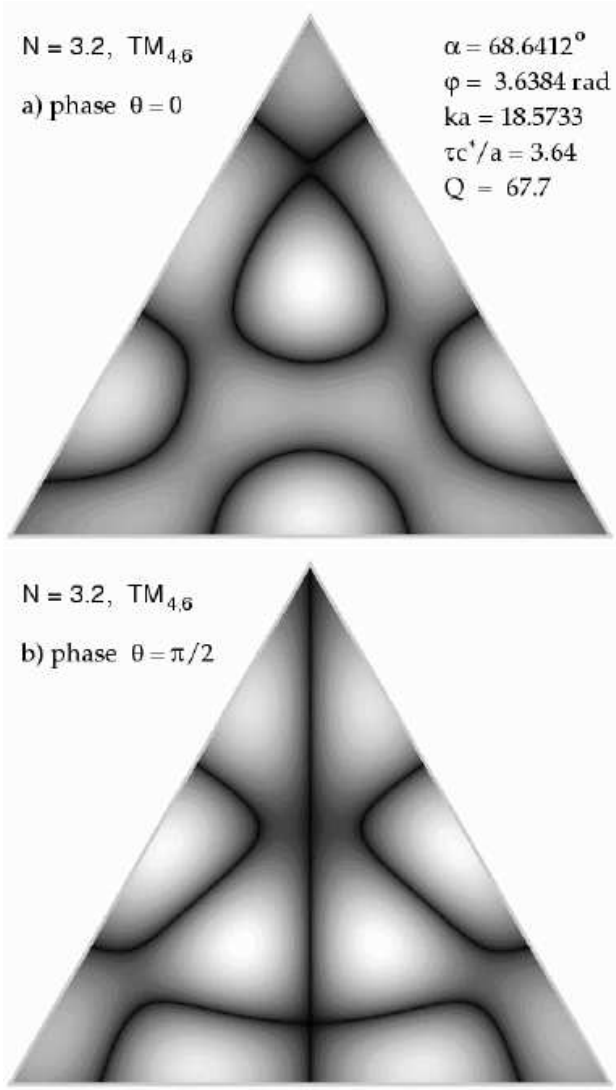

FIG. 8: First excited TM modes of oscillation at $\mathsf{N} = 3.2$, with $(m, n) = (4, 6)$, as described in Fig. 7. Two degenerate wavefunctions are displayed. In a) phase is $\theta_0 = 0$, in b) the phase is $\theta_0 = \pi/2$, where the mode amplitude is $A_0 = e^{i\theta_0}$, see text.

upper left, encompassing more of the possible modes from the DBC theory, down towards smaller m for a given n. An example of this is given in Fig. 6, showing the corresponding results for index ratio $\mathsf{N} = 8$. A larger number of states appears for each n, although the mode wavevectors have changed slightly.[19] Conversely, as N decreases below the value 2.0, the DBC-TIR upper limit passes the lower limit, leaving no modes that can be confined by TIR. Furthermore, as long as $\mathsf{N} > 2.0$, the total number of modes is not finite, since n can be adjusted to an adequately large value to reach the fundamental mode. The main effect of placing N very close to 2.0 will be to force the lowest frequency mode to a large value of ka and associated large minimum value of n.

The fundamental mode quantum indexes depend on N. At $\mathsf{N} = 3.2$, the fundamental mode has $(m, n) = (3, 5)$, and a diagram of its interior wavefunction ($\psi = E_z$) is shown in Fig. 7. The intensity of the pixels in these images has been set proportional to $|\mathrm{Re}\{\psi\}|^{1/2}$, rather than linear in $\mathrm{Re}\{\psi\}$, in order to sharpen the appearance of the zero crossings. The resulting nodal curves separate neighboring positive/negative regions of the wavefunctions. The calculation of mode lifetimes and quality factors indicated on the wavefunction diagrams is described later in Sec. IV C.

Wavefunctions for the first excited TM state at $\mathsf{N} = 3.2$, with $(m, n) = (4, 6)$, are shown in Fig. 8. It is important to note that for the TM modes, the fields have

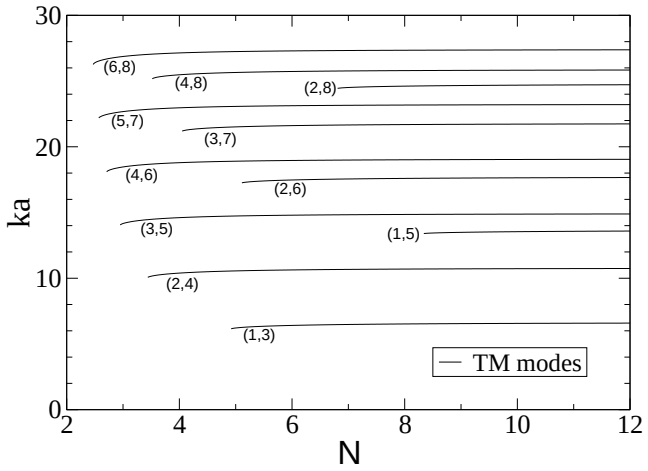

FIG. 9: TM mode wavevectors as functions of the index ratio N, for modes indicated by quantum indexes (m, n).

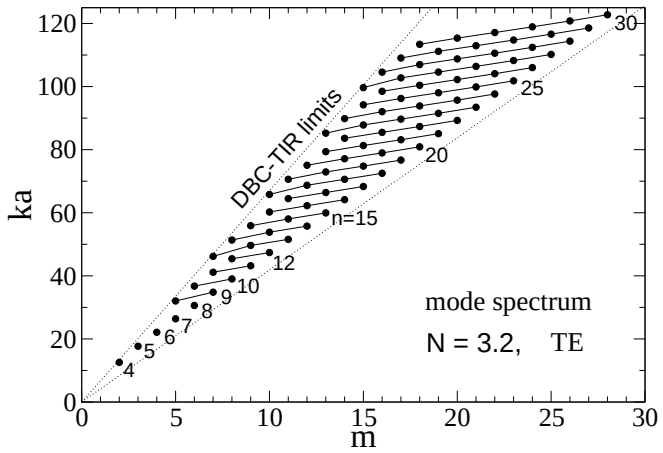

FIG. 10: The lowest mode wavevectors for TE polarization at index ratio N = 3.2, plotted as described in Fig. 5. The fundamental mode here has lower (m, n) and ka than that for TM polarization. On the other hand, at fixed (m, n), the mode wavevectors here are higher than those for TM polarization.

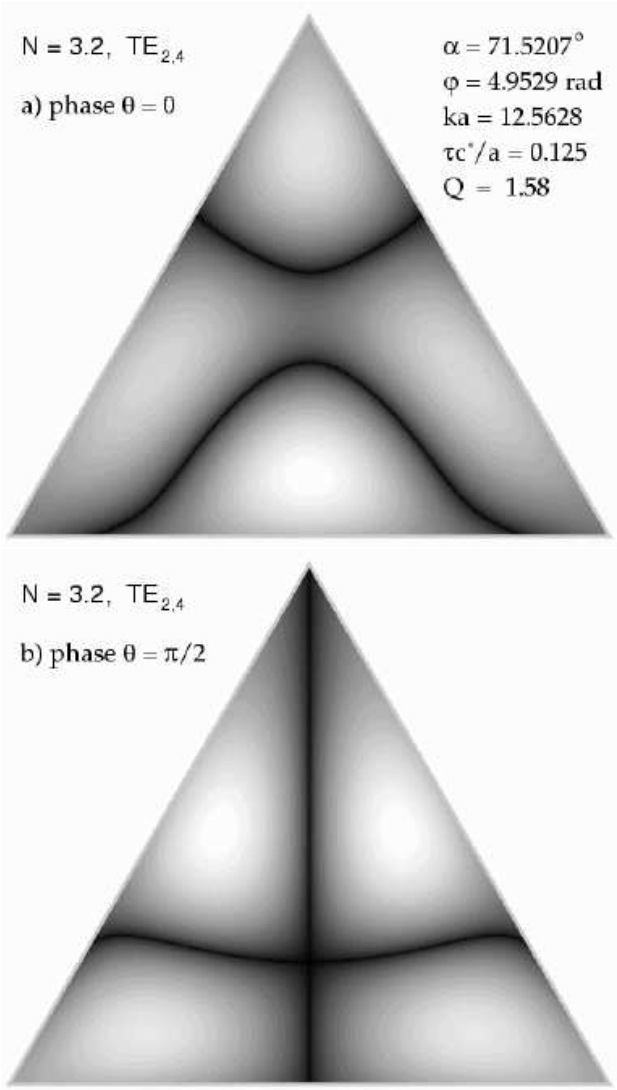

FIG. 11: Fundamental TE modes of oscillation at N = 3.2, with $(m, n) = (2, 4)$, as described in Fig. 7. Two degenerate wavefunctions are displayed. In a) phase is $\theta_0 = 0$, in b) the phase is $\theta_0 = \pi/2$, where the mode amplitude is $A_0 = e^{i\theta_0}$, see text.

substantial nonzero amplitudes even at the cavity edges. Furthermore, all these TIR-confined modes are doubly degenerate, since one can choose the two values $\pm k_x$ and form degenerate pairs of states. Alternatively, different degenerate wavefunctions can be obtained by putting the overall amplitude $A_0 = e^{i\theta_0}$, choosing some arbitrary phase θ_0, and using only the real part of (29). The degenerate pairs presented here were formed using $\theta_0 = 0$ and $\theta_0 = \pi/2$.

A rather weak dependence of some of the $\mathrm{TM}_{m,n}$ mode frequencies on index ratio is shown in Fig. 9. The cut-off index ratios appear clearly as the left termination points of each curve. These cutoffs are similar in magnitude to that from the DBC theory, rewriting Eq. (44),

$$\mathsf{N} > \mathsf{N}_c \equiv \sqrt{3\frac{n^2}{m^2} + 1}. \tag{47}$$

(See Fig. 13 for the DBC cutoffs.) However, the TM mode wavevectors are considerably lower than the prediction of the DBC theory, Eq. (35), because the TM reflection phase shifts $\delta_{i,l}$ are never near $-\pi$.

B. TE polarization

Results for the TE mode spectrum at N = 3.2 are shown in Fig. 10, in the same manner as displayed for TM

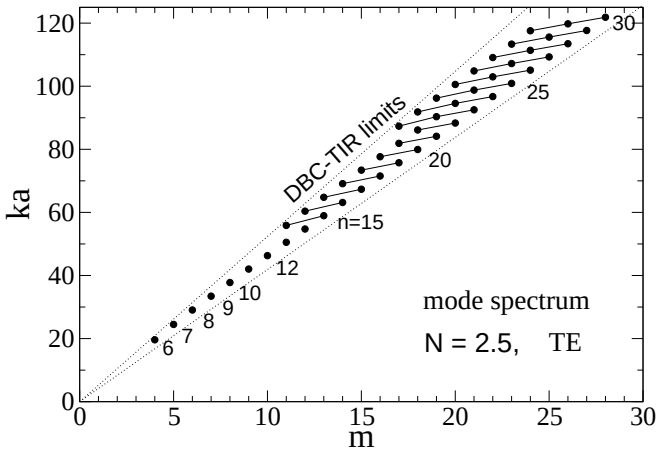

FIG. 12: The lowest mode wavevectors for TE polarization at index ratio N = 2.5, plotted as described in Fig. 5.

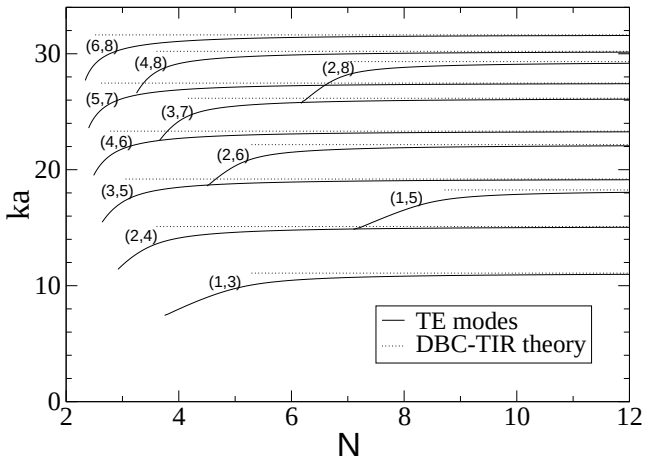

FIG. 13: TE mode wavevectors (solid curves) as functions of the index ratio N, for modes indicated by quantum indexes (m, n). The dotted lines show the DBC wavevectors, terminating at the cutoffs given by Eq. (47).

polarization. Again, the allowed mode indexes satisfy the parity constraint, and the ka values fall within the limits of the DBC-TIR theory. On the other hand, there are two primary differences compared to TM polarization. First, the fundamental mode has a lower (m, n) pair, and in addition, a slightly lower ka than for the fundamental mode with TM polarization. Second, at a given (m, n), we see that the wavevectors for TE polarization always are noticeably higher than for TM polarization.

At N = 3.2, the TE fundamental is $(m, n) = (2, 4)$, Fig. 11, however, the Q for this mode is extremely low, so that it cannot be considered stable.

In Fig. 12 we illustrate the effect of decreasing N down to the value 2.5, closer to the extreme limit 2.0 . Two low modes at $m = 4$ and $m = 5$ have been squeezed out by the lower DBC-TIR upper limit, as well as the entire spectrum becoming narrower. Of course, a similar squeezing effect takes places for the TM spectrum.

The dependence of some TE mode wavevectors on index ratio is shown in Fig. 13. Compared to the TM modes, the TE modes show a stronger variation with N, especially just above the cutoff ratio. The plot also shows the DBC mode wavevectors as dotted lines, terminating at the cutoffs predicted by the DBC-TIR theory, Eq. (47). Once N reaches adequately large values, the wavevectors from the calculations for dielectric boundary conditions asymptotically approach the DBC values. This can be attributed to the extra factor of ϵ/ϵ' in the TE phase shift formula (40), which easily causes all the reflection phase shifts to rapidly approach $-\pi$, the value under Dirichlet boundary conditions.

The fields diminish more rapidly near the cavity edges for TE polarization than for TM polarization. At N = 8.0, the fundamental modes have $(m, n) = (1, 3)$, whose corresponding wavefunction is the simplest possible, having a single nodal line across the cavity, Fig. 14. The avoidance of the fields close to the cavity boundaries of the TE mode is apparent, whereas, the TM fields tend towards maximum values near the boundaries.

Taken together, these results emphatically confirm the idea presented in Ref. 14 that the simple DBC theory is much more appropriate for TE polarization than for TM polarization.

C. Estimates of mode lifetimes due to boundary wave emission

The (doubly-degenerate) solutions found here are approximate. The assumption of evanescent traveling waves along each boundary, rotating around the triangle in the exterior region, is not exact, because the edges are of finite length. In reality, any of the evanescent waves can be expected to scatter from the triangle vertices, leading to radiation away from the cavity, and reflection of that evanescent wave backwards from the vertices. There should be linear combinations of evanescent traveling waves moving in both directions along the edges (standing waves). This in turn would lead to a mixing of the doubly degenerate modes, i.e., the degeneracy will be split due to the scattering experienced by the fields at the triangular vertices.

In the case of modes whose exterior wavelength is small compared to the cavity edge, these effects may be small, and ignoring the resulting degeneracy splitting, we can try to estimate the power loss, and hence, the mode lifetime. To accomplish this, following Wiersig[18], it is assumed that all the power in the evanescent boundary waves is radiated when reaching the vertices of the triangle, without reflecting backwards from the vertices. The lifetime τ and Q-factor are calculated by

$$\tau = U/P, \qquad Q = \omega\tau = 2\pi f\tau, \tag{48}$$

where U is the total energy in the cavity fields, and P is

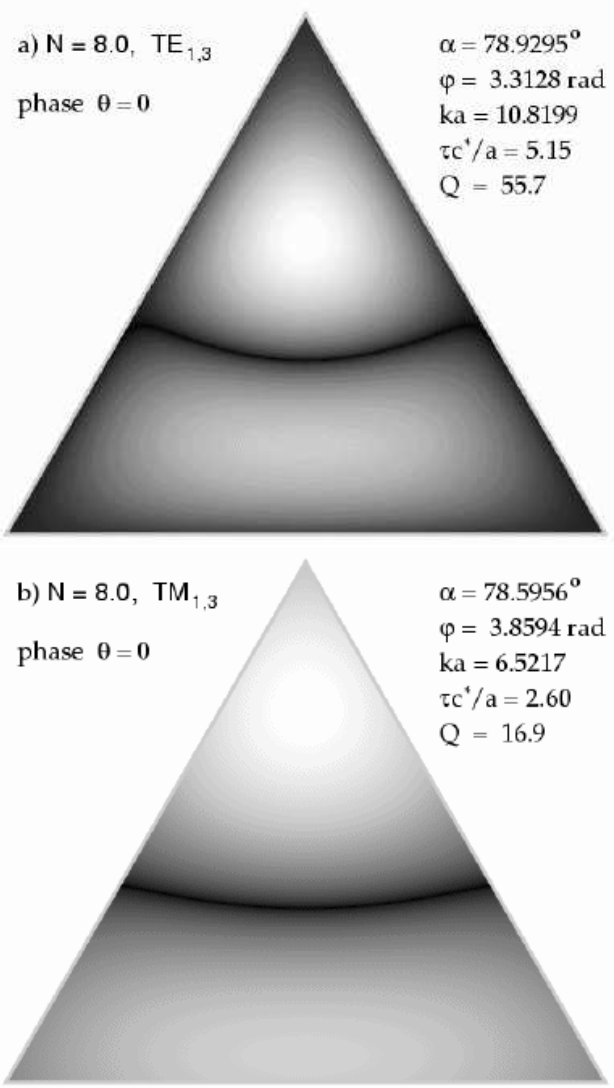

FIG. 14: Fundamental a) TE and b) TM modes of oscillation at $\mathsf{N} = 8.0$, with $(m, n) = (1, 3)$, as described in Fig. 7, both for phase $\theta = 0$, see text. (The choice $\theta = \pi/2$ would instead produce a vertical nodal line.)

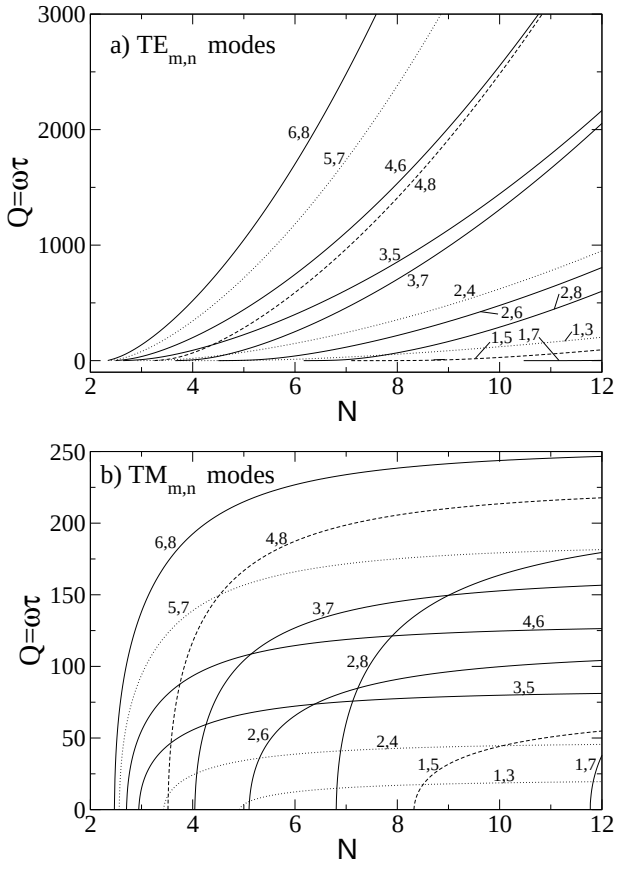

FIG. 15: Mode quality factors for a) TE and b) TM modes calculated from boundary wave emission, see (54) and (55), as functions of the index ratio N, with modes labeled by (m, n).

the total power radiated, as found from leakage of the evanescent boundary waves at the vertices. This approach was used also to estimate the mode lifetimes using the DBC solutions[14]; there it was found that generally speaking, the TE modes have longer lifetimes than the corresponding TM modes, provided the index ratio N is large. It is important to check the relative mode lifetimes using the more correct dielectric boundary conditions. As the present solution has demonstrated the avoidance of TE fields near the cavity boundaries, one might expect the TE lifetimes to be longer.

Following the calculations in Refs. 14, 18, the total energy of the fields in a cavity of height h can be written

$$U = \int h\ dx\ dy\ \frac{\epsilon|\vec{E}|^2}{8\pi} = \int h\ dx\ dy\ \frac{\mu|\vec{H}|^2}{8\pi}; \qquad (49)$$

the two forms convenient for TM modes ($|\vec{E}| = E_z = \psi$) and TE modes ($|\vec{H}| = H_z = \psi$), respectively. Using the wavefunction of Eq. (29), it is not possible to find a simple formula for this integral in the general case, thus it was evaluated by numerical integration within the triangle. In the DBC limit, with $\varphi = -\pi$, one finds $\int \frac{dx}{a}\frac{dy}{a}|\psi|^2 = 3\sqrt{3}|A_0|^2/8$; generally also for MBC the integral is of this order.

The total boundary wave power is taken as the sum of the powers from boundary waves on each edge. At each edge there are three different incident waves, each of which generates an evanescent wave. For example, on b_0, waves ③, ⑤ and ⑥ separately produce the evanescent waves ③′, ⑤′ and ⑥′. We sum the powers in each of these evanescent waves, then multiply by three due to triangular symmetry, to give the total power radiated.

The boundary wave power of an individual evanescent wave is calculated using the Poynting flux along the exterior side, $\vec{S}' = \frac{c}{8\pi}\mathrm{Re}\{\vec{E}' \times \vec{H}'^*\}$, expressed alternately

as

$$\vec{S}' = \frac{c}{8\pi\mu'}|\vec{E}\,'|^2 \mathsf{n}\sin\theta_i\,\hat{x} = \frac{c}{8\pi\epsilon'}|\vec{H}\,'|^2 \mathsf{n}\sin\theta_i\,\hat{x}, \quad (50)$$

where $\hat{x}$ points parallel to the boundary, and the incident angle from within the cavity is θ_i. The evanescent wave has an exponentially decaying behavior into the exterior medium. If A_i is the amplitude on the interior side, with boundary at $y = 0$, and the y-coordinate points from the boundary into medium n', Eqs. (9) and (37) give

$$|\psi\,'|^2 = |A_i[1 + e^{i\delta(\theta_i)}]e^{ik'_x x}e^{-k'\gamma' y}|^2. \quad (51)$$

Integrating the total flux contained from $y = 0$ to $y = \infty$ gives the power of this wave along the boundary, $P_x = h\int_0^\infty dy\ \vec{S}\,'\cdot\hat{x}$, with only a tiny formal difference for the two polarizations,

$$P_x = \frac{hc^2}{4\pi\omega}\frac{|A_i|^2\cos^2[\frac{1}{2}\delta(\theta_i)]}{\sqrt{1-(\sin\theta_c/\sin\theta_i)^2}} \times \begin{cases} \frac{1}{\mu'} & \text{(TM)}, \\ \frac{1}{\epsilon'} & \text{(TE)}. \end{cases} \quad (52)$$

In practice, however, the phase shifts for TE polarization are typically much closer to $-\pi$ than for TM polarization, which causes the TE powers to be smaller. The incident squared wave amplitude is $|A_i|^2 = \frac{1}{4}|A_0|^2$, as all the six wave components of ψ are of equal strength, Eq. (28).

The total emitted power from all edges is three times the sum of the powers on edge b_0,

$$P = 3(P_{x,3} + P_{x,5} + P_{x,6}). \quad (53)$$

Taking the net energy/power ratio and simplifying leads to the dimensionless lifetime expressions,

$$\frac{\tau c^*}{a} = \frac{\frac{2}{3}ka\int\frac{dx}{a}\frac{dy}{a}|\psi|^2}{\sum_{i=3,5,6}\frac{|A_0|^2\cos^2[\frac{1}{2}\delta_i]}{\sqrt{1-(\sin\theta_c/\sin\theta_i)^2}}} \times \begin{cases} \frac{\mu'}{\mu} & \text{(TM)}, \\ \frac{\epsilon'}{\epsilon} & \text{(TE)}. \end{cases} \quad (54)$$

The factor of $\epsilon'/\epsilon < 1$ for TE polarization tends to reduce the lifetime, however, the phase shifts in the denominator have an even larger effect, such that typically, the $\mathrm{TE}_{m,n}$ lifetime is found to be longer than the $\mathrm{TM}_{m,n}$ lifetime. The summation of power terms in the denominator is usually dominated by that of wave ⑥, which has the smallest incident angle. The expression is scaled by a/c^*, the time for the signal to cross the cavity. A well-defined mode should have $\tau c^*/a \gg 1$, however, usually it is more typical to look at the related mode quality factor, Q, defined by

$$Q = \omega\tau = c^* k\tau = (ka)(\tau c^*/a), \quad (55)$$

whihc is the dimensionless mode wavevector times the dimensionless lifetime.

Numerical results for Q versus index ratio are displayed for the lowest modes in Fig. 15, for TE and TM polarizations, assuming $\mu = \mu'$. One finds that Q's for TE modes are considerably larger than for TM modes, especially far enough above the cutoff N for a given mode.

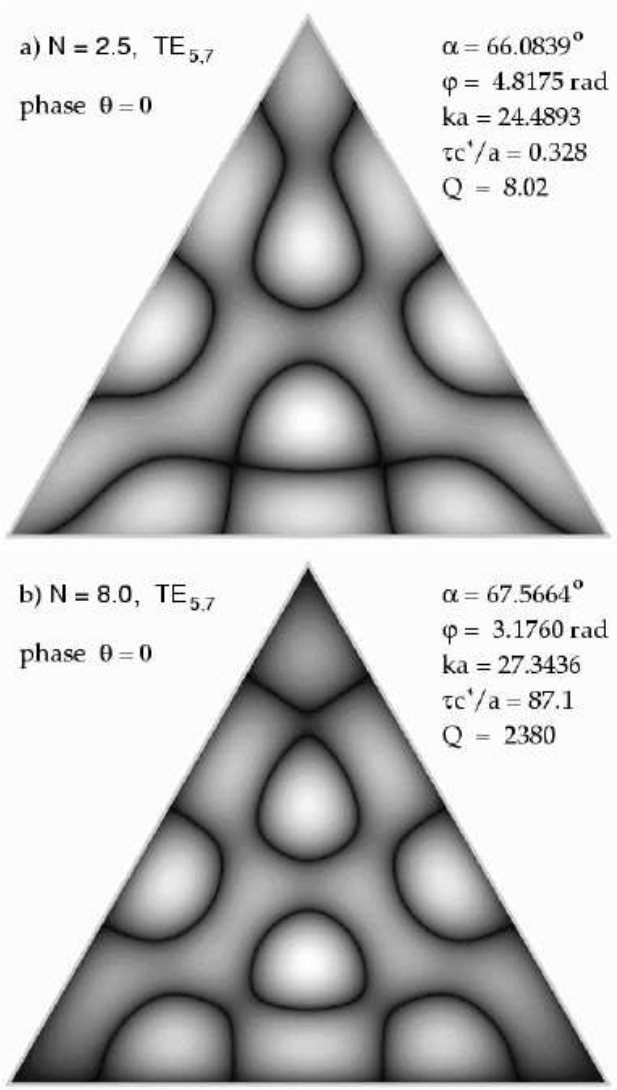

FIG. 16: Comparison of $\mathrm{TE}_{5,7}$ wavefunctions at a) $\mathsf{N} = 2.5$, only slightly above cutoff, and very weakly bound with small Q and b) $\mathsf{N} = 8.0$, substantially above the cutoff, with much higher Q, and field amplitude concentrated away from the boundaries.

Furthermore, the TM quality factors tend to saturate at large N, while the TE quality factors tend to increase proportional to $\mathsf{N}^2 = \epsilon/\epsilon'$. This latter effect can be seen due to the asymptotics for the TE reflection phase shift, based on the identity,

$$\cos^2\frac{\delta}{2} = \left(\frac{\epsilon'}{\epsilon}\right)^2 \frac{\cos^2\theta_i}{\sin^2\theta_i - \sin^2\theta_c + (\epsilon'/\epsilon)^2\cos^2\theta_i}. \quad (56)$$

The net result is that Q and τ for TE modes are proportional to ϵ/ϵ' in the limit of large index ratio, a factor not present for TM polarization.

It is interesting to observe the changes in the wavefunctions with increasing N or effectively, increasing Q. In Fig. 16, $\mathrm{TE}_{5,7}$ mode wavefunctions are plotted for $\mathsf{N} = 2.5$, just slightly above the cutoff index ratio, and

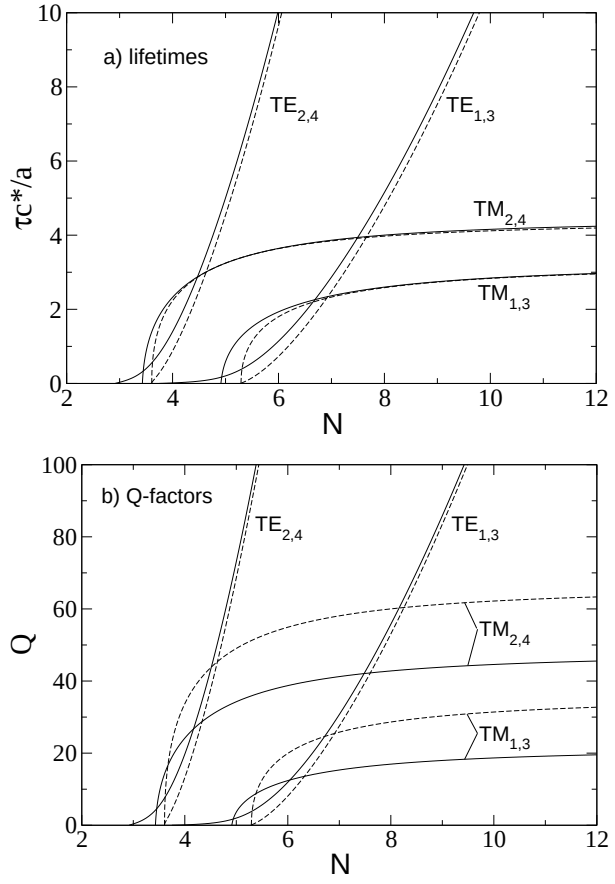

FIG. 17: Comparison of some mode a) lifetimes and b) quality factors, as functions of the index ratio N, from the present theory, using dielectric boundary conditions (solid curves), and from the simpler theory using Dirichlet boundary conditions (dashed curves). The modes are labeled by (m, n).

for N = 8, well above the cutoff. At lower N (and Q), a central lobe of ψ is connected to one vertex of the boundary, and another lobe is nearly coupled to the opposite edge. At higher N (and much higher Q), these interior lobes have become completely detached from the boundary, and the fields appear more concentrated within the interior, farther from the boundaries.

A comparison can be made between the results using dielectric boundary conditions and those from the simplified DBC theory[14]. Fig. 17 shows Q and τ results for the modes $(1, 3)$ and $(2, 4)$, as derived from the two approaches, using the total power in all boundary waves for this comparison. Indeed, there are only minor differences between the lifetimes, mostly near the cutoff index ratios, due to the fact that the DBC theory overestimates the cutoffs. For the quality factors, the discrepancy between the approaches is much greater for the TM modes, primarily because the DBC theory has overestimated their frequencies (or wavevectors). Nevertheless, the ability of the simplified DBC theory to predict the general trends with N is remarkable.

TABLE III: Properties of some of the lower TM mode for N = 3.2, labeled by (m, n) or by underlined indexes $(\underline{m}, \underline{l})$, where compared to results of Ref. 10, in parenthesis.

mode	α	ka	Q
$TM_{3,5}$	70.4167°	14.3406	32.18
$TM_{4,6\ (\underline{0},\underline{14})}$	68.6412°	18.5733 (18.8)	67.67
$TM_{5,7\ (\underline{0},\underline{16})}$	67.3705°	22.7686 (22.9)	107.9
$TM_{6,8\ (\underline{0},\underline{18})}$	66.4225°	26.9545 (27.0)	154.5
$TM_{7,9\ (\underline{0},\underline{20})}$	65.6894°	31.1374 (31.2)	207.9
$TM_{8,10\ (\underline{0},\underline{22})}$	65.1060°	35.3196 (35.3)	268.4
$TM_{6,10\ (\underline{1},\underline{21})}$	70.6463°	33.5168 (34.1)	145.8
$TM_{9,11\ (\underline{0},\underline{24})}$	64.6307°	39.5019 (39.5)	335.9
$TM_{7,11\ (\underline{1},\underline{23})}$	69.6339°	37.7112 (38.3)	227.4
$TM_{10,12}$	64.2363°	43.6845	410.4
$TM_{8,12}$	68.7916°	41.8887	307.3
...	...	...	...
$TM_{15,17\ (\underline{0},\underline{36})}$	62.9701°	64.6045 (64.5)	889.9 (15000)
$TM_{13,17\ (\underline{1},\underline{35})}$	66.1053°	62.7505 (62.9)	784.1 (4380)
$TM_{11,17}$	69.3950°	61.0455	593.5
$TM_{16,18\ (\underline{0},\underline{38})}$	62.8025°	68.7897 (68.7)	1007 (22000)
$TM_{14,18\ (\underline{1},\underline{37})}$	65.7527°	66.9250 (67.0)	899.0 (7000)
$TM_{12,18\ (\underline{2},\underline{36})}$	68.8431°	65.2085 (65.5)	717.7 (1230)
$TM_{17,19}$	62.6528°	72.9751	1132
$TM_{15,19}$	65.4386°	71.1006	1021
$TM_{13,19\ (\underline{2},\underline{38})}$	68.3516°	69.3713 (69.5)	845.1 (1960)

TABLE IV: Properties of some of the lower TE modes for N = 3.2, labeled by (m, n) or by underlined indexes $(\underline{m}, \underline{l})$, where compared to results of Ref. 10, in parenthesis.

mode	α	ka	Q
$TE_{2,4}$	71.5207°	12.5628	1.576
$TE_{3,5}$	69.9852°	17.6896	18.95
$TE_{4,6}$	68.4450°	22.1165	60.13
$TE_{5,7\ (\underline{0},\underline{16})}$	67.2586°	26.3873 (26.2)	121.4
$TE_{6,8}$	66.3498°	30.6105	200.1
$TE_{7,9}$	65.6382°	34.8149	294.6
$TE_{5,9}$	71.3190°	32.0399	15.63
$TE_{8,10\ (\underline{0},\underline{22})}$	65.0678°	39.0107 (39.0)	404.1
$TE_{6,10}$	70.3771°	36.7552	59.80
...	...	...	...
$TE_{14,16\ (\underline{0},\underline{34})}$	63.1471°	64.1404 (64.2)	1350 (6130)
$TE_{12,16\ (\underline{1},\underline{33})}$	66.4654°	62.2279 (62.4)	789 (4100)
$TE_{10,16}$	69.8843°	60.2288	221
$TE_{15,17\ (\underline{0},\underline{36}}$	62.9597°	68.3271 (68.4)	1560 (10860)
$TE_{13,17\ (\underline{1},\underline{35})}$	66.0736°	66.4147 (66.6)	972 (15320)
$TE_{11,17}$	69.2967°	64.4910	346

D. Comparison with other ETR theory for dielectric boundary conditions

ETR modes have previously been analyzed by Huang *et al.*(HGW)[10] using different approximations, also involving matching of interior fields undergoing TIR to exterior evanescent fields. In particular, HGW used what was called a "perfectly confined approximation for the transverse wavefunction." This is a Dirichlet boundary condition on part of the full wavefunction, giving the y-component of wavevector ① [Eq. (9) of Ref. 10],

$$k_y a = \frac{2\pi}{\sqrt{3}}(\underline{m}+1), \qquad \underline{m} = 0, 1, 2, \ldots \tag{57}$$

Indeed, this is the same as Eq. (32) reviewed here for the DBC problem, with $\underline{m}+1$ equivalent to $n = n_6 + 2$. Thus, it is noticeably different from the result for dielectric boundary conditions, Eq. (23b), which more fully accounts for all the reflection phase shifts. The factor $\underline{m}+1$ begins at the value 1, whereas, in our results, the minimum value of equivalent quantum index n is 3. For the other component of wavevector ①, the result obtained [Eq. (21) of Ref. 10] is similar to Eq. (23a),

$$k_x a = \frac{2\pi}{3}\underline{l} - 2\underline{\theta}, \qquad \underline{l} = 3, 4, 5, \ldots \tag{58}$$

where $\underline{l}$ has the same parity as $\underline{m}$, and $\underline{\theta}$ is an individual TIR Fresnel phase shift, having different forms for TM and TE modes. Index $\underline{l}$ appears equivalent to $m = n_3 - n_5$, however, Eq. (23a) involves phase shifts of two different waves, instead of the individual phase shift $\underline{\theta}$.

For a chosen value of n, different choices of m give solutions with ka of similar magnitude, like the modes connected by solid lines in Figs. 5, 6, 10 and 12. This "number of transverse modes" increases with both n and N, and is smaller than that found in Ref. 10. Because $ka = 2\pi\mathsf{N}/\lambda$ depends on (m, n) in a nontrivial way, it is not possible to give a simple expression for this mode count.

For $\mathsf{N} = 3.2$, a summary is made of the lowest TM and TE modes in Tables III and IV and compared to results from HGW. In spite of the obvious differences in these theoretical approaches, they both lead to very similar predictions for the mode wavevectors or frequencies, agreeing to within about one percent. The prediction of the Q-values are considerably different; HGW used the finite-difference time-domain (FDTD) technique[13] combined with Padé approximates to estimate Q. In particular, the FDTD technique predicts that TE polarization results in much smaller Q than TM polarization[11], exactly opposite to our results (Fig. 15). The short lifetime for TE modes was explained by the zero in the reflectivity at the Brewster angle θ_B, which is only slightly less than the critical angle. However, in a confined TIR wavefunction, all six plane wave components must impinge on the faces at angles greater than θ_c and hence greater than θ_B, so it is hard to understand how the Brewster minimum comes into play, unless diffractive effects at the triangle vertices are strong, causing violation of the six-wave assumption.

TABLE V: Mode frequencies and free space wavelengths in the range around 1.3 to 1.6 μm, for cavities with $\mathsf{N} = 3.2$ and edge lengths a. The modes are labeled by m, n. Wavelengths marked with an asterisk fall about 2% below peaks in PL data, Ref. 3

a (μm)	mode	ka	λ (μm)	f (THz)
2	$TM_{3,5}$	14.341	1.5675	191.25
2	$TE_{1,3}$	12.563	1.7893	167.54
5	$TM_{6,10}$	33.517	1.6767	178.79
5	$TM_{8,10}$	35.320	1.5911*	188.41
5	$TM_{7,11}$	37.711	1.4902*	201.17
5	$TM_{9,11}$	39.502	1.4227*	210.72
5	$TM_{8,12}$	41.889	1.3416*	223.46
5	$TM_{10,12}$	43.685	1.2865*	233.03
5	$TE_{5,9}$	32.040	1.7540	170.92
5	$TE_{7,9}$	34.815	1.6142	185.72
5	$TE_{6,10}$	36.755	1.5290	196.07
5	$TE_{8,10}$	39.011	1.4406	208.10
5	$TE_{7,11}$	41.135	1.3662	219.43
5	$TE_{9,11}$	43.202	1.3008	230.46

E. Mode generation near 1.55 μm free space wavelength

There has been recent interest, both experimental and theoretical, in using semiconductor ETRs operating around 1.55 μ m wavelength. [3, 10, 11, 17] Here we assume a cavity medium with $\mathsf{n} = 3.2$, surrounded by vacuum, and summarize the mode spectra obtained by the present theory, for some typical cavity edge lengths, $a = 2\mu$m and $a = 5\mu$m. Of course, all mode frequencies simply scale as $1/a$, thereby giving the primary tuning control parameter. Modes whose wavelength outside the cavity ranging from approximately 1.30μm to 1.60μm are considered; this corresponds to frequency range 187 THz $< f <$ 231 THz.

Results for all the modes found from 1.3 to 1.6 μm are shown in Table V for TM and TE polarization. Obviously very few modes occur in any such narrow range if the cavity is small ($a = 2\mu$m), which could allow for fine frequency tuning. Conversely, many modes are present in larger cavities (such as $a = 10\mu$m) and single mode operation is difficult. A cavity with $a = 5\mu$m has a moderate number of modes; the TM mode wavelengths are similar to those found in photoluminescence (PL) experiments[3]. In fact, five of TM mode wavelengths calculated here are about 2% lower than five peaks seen in Fig. 2 of Ref. 3. This deviation might be attributed

primarily to an uncertainty in the cavity size, and secondly, caused by a weak variation of dielectric constant with wavelength.[3] Discounting these factors, the agreement for the 5μm cavity is reasonable. Comparison with the experimental spectrum for $a = 10\mu$m is more difficult, although it appears that some of the $\mathrm{TM}_{m,m+2}$ modes from the present theory (not shown) do appear in the PL data, again allowing for uncertainty in a and dispersion.

V. CONCLUSIONS

The phase relationships between the six plane waves within an ETR have been determined so they match correctly to each other and to exterior evanescent waves, according to Fresnel reflection coefficients for a dielectric on dielectric boundary at index ratio $\mathsf{N} = \mathsf{n}/\mathsf{n}'$. The theoretical wavefunction description is actually very general; it applies to any choice of reflection phase shifts, including those for DBC, and TE or TM polarizations. The main approximation here has been that the evanescent fields do not perturb the interior fields; assuming the evanescent fields radiate at the triangle vertices (a strong damping approximation), the mode lifetimes and quality factors have been estimated. Modes with high Q should be very well described by the wavefunction (29). The mode wavevectors are consistent with previous analyses [10, 11, 17], although the wavefunction description and quality factors differ from the FDTD technique[11] results. Some mode results are consistent with PL experimental data on 5μm semiconductor ETRs[3].

For N adequately above the cutoff for a mode (m, n), the TE mode wavevectors are very close to the predictions from the simplified DBC theory, whereas, the TM mode wavevectors are consistently below the DBC results. This is because large N results in Fresnel reflection phase shifts very near $-\pi$, the value for the DBC theory, only for TE polarization. This causes the TE wavefunctions to avoid the cavity edges; on the other hand, the TM wavefunctions have significant amplitude at the edges. For both polarizations, dielectric boundary conditions give lower cutoff index ratios than from the DBC theory. As N increases starting from 2.0, the theory demonstrates how the spectrum of available modes expands (Fig. 5, etc.), but always stays within the limits predicted from the DBC theory.

An extra factor of ϵ/ϵ' appears in the lifetime for TE modes, not present for TM modes. This theory then predicts considerably larger lifetimes and Q's for TE polarization, whereas the FDTD approach[11] led to larger Qs for TM modes. At large index ratio, the lifetimes found here approach the values found in the simpler DBC theory[14], for both polarizations.

Acknowledgments

The author is grateful for discussions with Wagner Figueiredo and Luis G. C. Rego and their hospitality at the Universidade Federal de Santa Catarina, Florianópolis, Brazil, where this work was completed.

[1] S. L. McCall, A. F. J. Levi, R. E. Slusher, S. J. Pearton, and R. A. Logan, Appl. Phys. Lett. **60**, 289 (1992).
[2] H. C. Chang, G. Kioseoglou, E. H. Lee, J. Haetty, M. H. Na, Y. Xuan, H. Luo, A. Petrou, and A. N. Cartwright, Phys. Rev. **A 62**, 013816 (2000).
[3] Q. Y. Lu, X. H. Chen, W. H. Guo, L. J. Yu, Y. Z. Huang, J. Wang, and Y. Luo, IEEE Phot. Tech. Lett. **16**, 359 (2004).
[4] A. W. Poon, F. Courvoisier, and R. K. Chang, Opt. Lett. **26**, 632 (2001).
[5] C. Y. Fong and A. W. Poon, Optics Express **11**, 2897 (2003).
[6] H.-J. Moon, K. An, and J.-H. Lee, Appl. Phys. Lett. **82**, 2963 (2003).
[7] U. Vietze, O. Krauß, F. Laeri, G. Ihlein, F. Schüth, B. Limburg, and M. Abraham, Phys. Rev. Lett. **81**, 4628 (1998).
[8] I. Braun, G. Ihlein, F. Laeri, J. U. Nöckel, G. Schulz-Ekloff, F. Schüth, U. Vietze, O. Weiß, and D. Wöhrle, Appl. Phys. B: Lasers Opt. **B 70**, 335 (2000).
[9] M. G. Lamé, *Leçons sur la théorie mathématique de l'élasticité des corps solides* (Bachelier, Paris, 1852).
[10] Y. Z. Huang, W. H. Guo, and Q. M. Wang, IEEE J. Quan. Elec. **37**, 100 (2001).
[11] W. H. Guo, Y. Z. Huang, and Q. M. Wang, IEEE Phot. Tech. Lett. **12**, 813 (2000).
[12] Y. Z. Huang, Proc. SPIE **3899**, 239 (1999).
[13] S. Dey and R. Mittra, IEEE Microwave and Guided Wave Lett. **8**, 415 (1998).
[14] G. M. Wysin, J. Opt. A: Pure Appl. Opt. **7**, 000000 (July, 2005).
[15] M. Brack and R. K. Bhaduri, *Semiclassical Physics* (Addison-Wesley Frontiers in Physics, 1997).
[16] J. D. Jackson, *Classical Electrodynamics* (John Wiley and Sons, New York, 1975), 2nd ed.
[17] Y. Z. Huang, W. H. Guo, L.-J. Yu, and H.-B. Lei, IEEE J. Quan. Elec. **37**, 1259 (2001).
[18] J. Wiersig, Phys. Rev. A **67**, 023807 (2003).
[19] The mode frequencies, given by $\omega = ck/\mathsf{n}$, may or may not diminish with increasing N, depending on whether N changed due to increased n or due to decreased n'.